Article

Potential for large-scale CO_2 removal via enhanced rock weathering with croplands

Check for updates

David J. Beerling[1 ✉], Euripides P. Kantzas[1], Mark R. Lomas[1], Peter Wade[1], Rafael M. Eufrasio[2], Phil Renforth[3], Binoy Sarkar[4], M. Grace Andrews[5], Rachael H. James[5], Christopher R. Pearce[6], Jean-Francois Mercure[7,8], Hector Pollitt[8,9], Philip B. Holden[10], Neil R. Edwards[8,10], Madhu Khanna[11], Lenny Koh[2], Shaun Quegan[12], Nick F. Pidgeon[13], Ivan A. Janssens[14], James Hansen[15] & Steven A. Banwart[16,17]

Enhanced silicate rock weathering (ERW), deployable with croplands, has potential use for atmospheric carbon dioxide (CO_2) removal (CDR), which is now necessary to mitigate anthropogenic climate change[1]. ERW also has possible co-benefits for improved food and soil security, and reduced ocean acidification[2–4]. Here we use an integrated performance modelling approach to make an initial techno-economic assessment for 2050, quantifying how CDR potential and costs vary among nations in relation to business-as-usual energy policies and policies consistent with limiting future warming to 2 degrees Celsius[5]. China, India, the USA and Brazil have great potential to help achieve average global CDR goals of 0.5 to 2 gigatonnes of carbon dioxide (CO_2) per year with extraction costs of approximately US\$80–180 per tonne of CO_2. These goals and costs are robust, regardless of future energy policies. Deployment within existing croplands offers opportunities to align agriculture and climate policy. However, success will depend upon overcoming political and social inertia to develop regulatory and incentive frameworks. We discuss the challenges and opportunities of ERW deployment, including the potential for excess industrial silicate materials (basalt mine overburden, concrete, and iron and steel slag) to obviate the need for new mining, as well as uncertainties in soil weathering rates and land–ocean transfer of weathered products.

The failure of the world to curb fossil fuel CO_2 emissions[6], and the inadequacy of planned mitigation measures[7], has been greeted with growing public consternation[8] consistent with the intergenerational injustice of human-caused climate change[9]. Even the most ambitious emission phase-outs[9,10] fail to achieve the United Nations Framework Convention on Climate Change Paris Agreement targets for limiting global warming without the help of massive amounts of atmospheric CDR. Extraction goals[1,7,9,10] later this century in most studies are on the order of at least 10 gigatonnes of CO_2 per year (Gt CO_2 yr^{-1}), although projections of rapid technological change[5] suggest a lower requirement of 2–2.5 Gt CO_2 yr^{-1}. This formidable challenge has led to international calls for urgent research into a portfolio of CDR options to understand their feasibility, scope, costs and challenges[11,12].

Our focus is terrestrial ERW, a CDR strategy based on amending soils with crushed calcium- and magnesium-rich silicate rocks to accelerate CO_2 sequestration[2–4,13–17]. Basalt, an abundant fast-weathering

rock with the required mineral chemistry, could be ideal for implementing land-based ERW because of its potential co-benefits for crop production[18] and soil health[2–4]. ERW liberates base cations, generating alkalinity, so that atmospheric CO_2 is converted into dissolved inorganic carbon (principally hydrogen carbonate ions; HCO_3^-) that is removed via soil drainage waters. These weathering products are transported via land surface runoff to the oceans with a storage lifetime exceeding 100,000 years[19]. Depending on soil type and pH, atmospheric CO_2-derived dissolved inorganic carbon may also be sequestered through the formation of soil carbonate minerals, which reduces the efficiency of carbon sequestration by approximately half[19]. The logistical infrastructure to apply basaltic rock dust to managed croplands already exists owing to the common need to apply crushed limestone to reverse soil acidification resulting from intensive cropping[2–4]. Thus, rapid deployment at large scale appears to be feasible within decades, and has important ancillary benefits including mitigation of
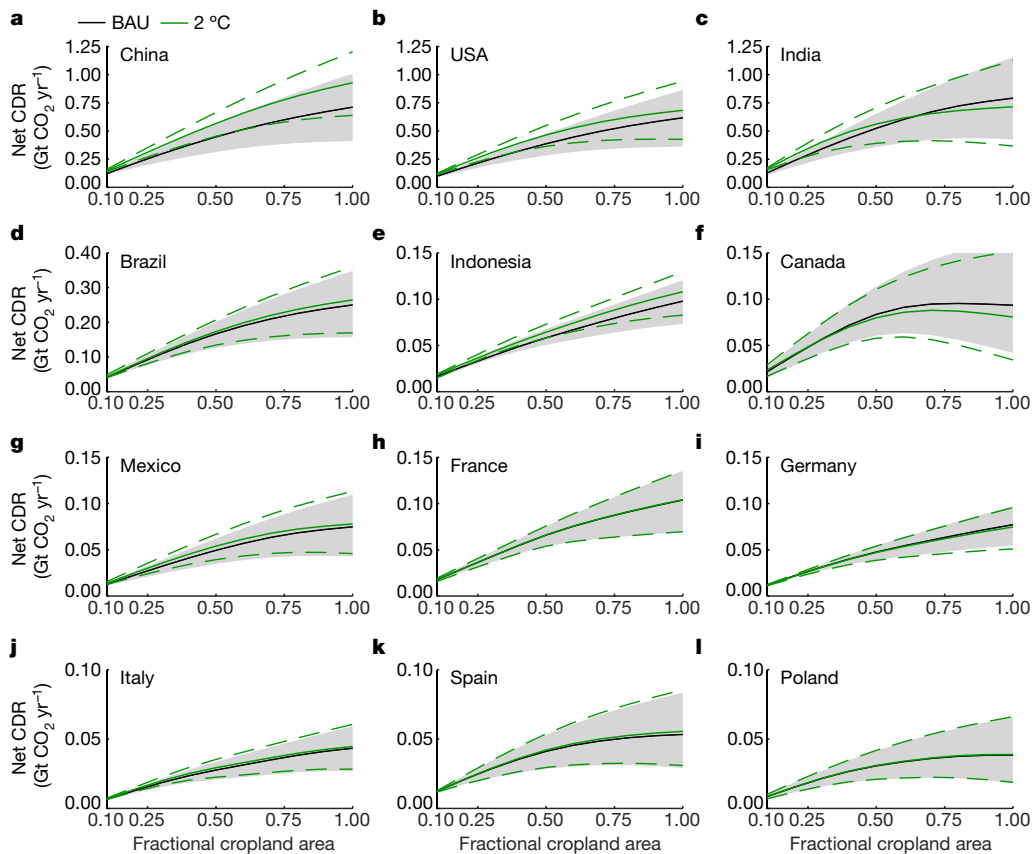
Fig. 1 | CDR via ERW with croplands. Net CDR curves for nations with the highest CDR potential worldwide (**a**–**g**) and in Europe (**h**–**l**) as a function of increasing ERW deployment across existing croplands. Note the y-axis scale changes. Results are shown for the BAU and the 2 °C energy policy scenarios. The grey-shaded area for each nation represents the 90% confidence interval calculated for basalts with relatively slow- versus fast-weathering rates for the BAU scenario; short green dashed lines indicate the 90% confidence limits of the corresponding 2 °C scenario simulations. Uncertainty in net CDR increases as ERW deploys onto croplands occupying a wider range of environmental conditions.

ocean acidification[15–18]. Carbon sequestration by ERW on croplands—a biogeochemical CDR option supporting multiple United Nations sustainable development goals and ecosystem services[4,20], and a pragmatic land-use choice to maximize scalability and co-benefits—thus warrants detailed examination.

We constructed a performance model with sub-national level of detail to assess quantitatively the CDR capacity and costs for land-based ERW implementation in major economies, constrained by available agricultural land area and energy production (including USA, India, China, Brazil and Europe) (Extended Data Fig. 1). For rock weathering within the soil profile, we developed a one-dimensional vertical reactive transport model with steady-state flow, and a source term representing rock grain dissolution (Methods; Supplementary Figs. 1–12; Supplementary Tables 1–5). Our work builds on advances made in prior ERW research largely on tropical forested ecosystems[15–17,21,22], with the practical aims of understanding the capacity of agriculture to capture carbon via soil amendment with milled basalt. For this initial nation-by-nation assessment, we examine the sensitivity of net CDR on current croplands to the projected national energy production for 2050 under a business-as-usual (BAU) energy scenario based on ongoing energy transitions[5]. This is compared with a 2 °C scenario (that is, a scenario in which the increase in global mean temperature since the pre-industrial period is limited to 2 °C by 2050), which includes a wide range of policy measures designed to respect the 2 °C target with 75% probability[5] (Supplementary Tables 6–12).

CDR potential via ERW

Our geospatial analyses define a new technical potential CDR range for those nations with high capacity for ERW deployment on cropland (Fig. 1; Supplementary Figs. 13–15). For each nation, we generate CO_2 capture curves by ranking CDR potential from the highest to the lowest grid cells with increasing ERW deployment. National median CDR curves typically show CDR capacity rising with increasing cropland area,

with CDR by silicate soil amendment reaching a plateau, or declining in the case of Canada (Fig. 1). These patterns reflect expansion of ERW into climatically unfavourable agricultural land, causing CDR potential to slow relative to the carbon penalty of logistical operations, and our assumed 3% limit in national energy available for grinding (see Methods section 'Cost assessments' and Extended Data Fig. 2). Overall trends in national CDR curves are relatively insensitive to the choice of energy scenario. China is the exception because its large increase in low-carbon energy usage projected under the 2 °C scenario[5] allows net CDR to rise by substantially reducing secondary CO_2 emissions from logistical operations (Fig. 1). This contrasts with results for India, whose total energy production falls by around 40% with a transition to low-carbon energy production in the 2 °C scenario, lowering the energy available for grinding basalt, and thus the potential for increased CDR by ERW. Reductions in energy production for other nations in the 2 °C scenario compared with the BAU scenario similarly lower their potential for increased CDR with the transition to low-carbon energy.

Recognizing the urgent need to assess large-scale options for meeting near-term CDR goals[10], we determine the potential contribution of nations to achieve CDR goals across the 0.5–2 Gt CO_2 yr^{−1} range (Table 1; Extended Data Fig. 3). Overall, we find that the three countries with the highest CDR potential are coincidentally the highest fossil fuel CO_2 emitters (China, USA and India)[6] (Fig. 1). Indonesia and Brazil, with CO_2 emissions 10–20 times lower than the USA and China, have relatively high CDR potential owing to their extensive agricultural lands and warm, seasonally wet climates conducive to high silicate rock weathering efficiency. European countries have a CDR potential an order of magnitude lower than those of China, USA and India, mainly because of less agricultural land area. The five European nations with the highest net CDR potential could offset 30% of the current emissions of European nations in 2019 and the three European countries with the highest CDR potential are also the largest European emitters of CO_2 from fossil fuels (Germany, Spain and Poland)[6]. Our ERW scenarios (Table 1) correspond to an aggregate CDR of 25–100 Gt CO_2

Article

if sustained over five decades. This would save up to 12% of the remaining cumulative carbon emission budget (about 800 Gt CO_2) that gives a 66% probability of limiting global warming to below 2 °C above the pre-industrial average surface temperature[10].

In the context of our CDR goals, ERW has a potential similar to that of other CDR strategies[23] estimated for 2050, including bio-energy with carbon capture and storage (BECCS), widely adopted in IPCC future scenarios (0.5–5 Gt CO_2 yr^{-1}), direct air capture and storage (DAC) (0.5–5 Gt CO_2 yr^{-1}), biochar (0.5–2 Gt CO_2 yr^{-1}), soil organic carbon sequestration (0.5–5 Gt CO_2 yr^{-1}), and afforestation/reforestation (0.5–3.6 Gt CO_2 yr^{-1}). One benefit of country-level analysis for CDR is the scope for comparative assessments with other technologies and opportunities for co-deployment. For example, our ERW CDR range is comparable with large-scale implementation of BECCS in the USA by 2040 (0.3–0.6 Gt CO_2 yr^{-1}), as constrained by biomass productivity, location and capacity of CO_2 storage sites[24]. ERW avoids competition for land used in food production, and related increased demands of BECCS for freshwater and polluting fertilizers[25], with CO_2 being treated as a resource for mineral weathering. Co-deployment of ERW with feedstock crops for BECCS and biochar could enhance the feasibility and carbon sequestration potential of these strategies[4,26].

Inorganic carbon sequestration by ERW appears to be comparable to soil organic carbon sequestration, another proposed CDR strategy (about 2.5 Gt CO_2 yr^{-1} by 2100)[27] using agricultural land, but with potentially greater long-term security of carbon storage. Co-deployment of ERW and soil organic carbon sequestration at large scale might, therefore, contribute substantially to the 5 Gt CO_2 yr^{-1} CDR goal suggested in decarbonization scenarios[10] for 2050. Compatibility of ERW and soil organic carbon sequestration may be realistic given that amendment of acidic organic-rich soils with silicate minerals, and the resultant pH increase, had no effect on respiratory CO_2 fluxes[28,29], contrary to concerns that increased soil pH may accelerate organic matter decomposition[30]. However, efficacy of CDR, sink saturation, and permanency of storage with these approaches, separately and interactively, are uncertain[11,23]. Abatement of soil N_2O emissions by basalt application to conventionally managed arable and perennial crops[31], and of N_2O and CH_4 emissions by application of artificial silicates to rice agriculture[32], is possible. Such effects would further lower adverse impacts of agriculture on climate per unit yield, amplifying the climate mitigation potential of ERW.

Greenhouse gas emissions reductions aimed at limiting future warming are defined under the Paris Agreement by Nationally Determined Contributions (NDCs)[33]. As yet, most of the top ten fossil carbon emitting nations are failing to meet their 2030 NDC pledges which, even if met, imply a median global warming (2.6–3.1 °C) exceeding the Paris agreement[33]. Warming of this magnitude could allow the Earth system to cross thresholds for irreversible planetary heating and long-term multi-metre sea-level rise, with potentially disastrous consequences for coastal cities[34]. NDC pledged carbon emission reductions undergo periodic revision in response to trends in greenhouse gas emissions, uptake of low-carbon energy technology, and climate[33] and hence are not set for 2050. We therefore illustrate the potential for undertaking ERW with agricultural lands to strengthen near-term national 2030 NDCs (Fig. 2).

Results show that China may be able to augment its pledged 2030 NDCs by about 5% to 10%, with similar gains for the USA, which has opted out of the Paris agreement. For India, the gain rises to 40% of its current pledged emissions, and Brazil may be able to offset 100% of its pledged 2030 CO_2 emissions plus some fraction of those from other countries (Fig. 2). Other countries outside Europe considered in our analysis (Indonesia, Canada, Mexico) may be able to augment their NDCs by up to 30% (Fig. 2). In Europe, ERW could aid substantial decarbonization of France and Spain (up to approximately 40%), and to a lesser extent Poland, Italy and Germany (all about 10%) (Fig. 2). ERW, therefore, may have a role to play in compensating for residual carbon

Table 1 | CDR goals for ERW with croplands in 2050

Goal		Cropland area (%)	National CDR (Gt CO_2 yr^{-1})	Silicate demand (Gt yr^{-1})	Cost (US$ per t CO_2 yr^{-1})
0.5 Gt CO_2 yr^{-1}					
World	China	10	0.13	0.77	102.1
	USA	11	0.11	0.63	160.3
	India	11	0.15	0.84	78.4
	Brazil	10	0.041	0.22	123.8
	Indonesia	10	0.017	0.091	54.3
	Canada	10	0.022	0.13	177.6
	Mexico	10	0.013	0.073	97.5
Europe	France	10	0.017	0.085	158.1
	Germany	11	0.012	0.066	167.8
	Italy	11	0.0070	0.039	181.9
	Spain	10	0.012	0.066	192.8
	Poland	10	0.0085	0.050	171.6
1.0 Gt CO_2 yr^{-1}					
World	China	23	0.26	1.59	109.3
	USA	24	0.21	1.26	168.5
	India	23	0.24	1.50	79.9
	Brazil	23	0.083	0.45	116.4
	Indonesia	25	0.033	0.18	57.5
	Canada	16	0.030	0.20	191.7
	Mexico	23	0.025	0.15	103.1
Europe	France	24	0.034	0.17	160.4
	Germany	25	0.025	0.14	171.7
	Italy	23	0.014	0.083	191.0
	Spain	17	0.018	0.10	190.9
	Poland	17	0.012	0.081	170.9
1.5 Gt CO_2 yr^{-1}					
World	China	38	0.40	2.48	114.5
	USA	39	0.32	1.99	173.1
	India	36	0.37	2.35	80.2
	Brazil	36	0.13	0.71	110.5
	Indonesia	41	0.050	0.28	58.6
	Canada	25	0.045	0.35	207.3
	Mexico	37	0.038	0.23	105.6
Europe	France	38	0.050	0.26	159.5
	Germany	39	0.037	0.20	173.6
	Italy	37	0.021	0.13	194.1
	Spain	28	0.026	0.17	189.3
	Poland	27	0.019	0.13	171.3
2.0 Gt CO_2 yr^{-1}					
World	China	55	0.53	3.46	120.7
	USA	55	0.42	2.72	176.7
	India	51	0.49	3.30	80.9
	Brazil	51	0.17	0.98	106.2
	Indonesia	59	0.067	0.38	59.4
	Canada	35	0.060	0.51	220.3
	Mexico	52	0.050	0.33	106.8
Europe	France	54	0.067	0.36	157.1
	Germany	57	0.050	0.28	175.9
	Italy	55	0.029	0.18	193.3
	Spain	41	0.035	0.25	190.7
	Poland	38	0.025	0.19	175.4

All values are means of both energy scenarios; see main text for details. For each country, c, we assigned its contribution, CDR(c), to a global CDR goal as follows, where CDR$_{max}$(c) is the maximum CDR value attainable by a country: $CDR(c) = CDR_{goal} \frac{CDR_{max}(c)}{\sum_{countries} CDR_{max}(c)}$.
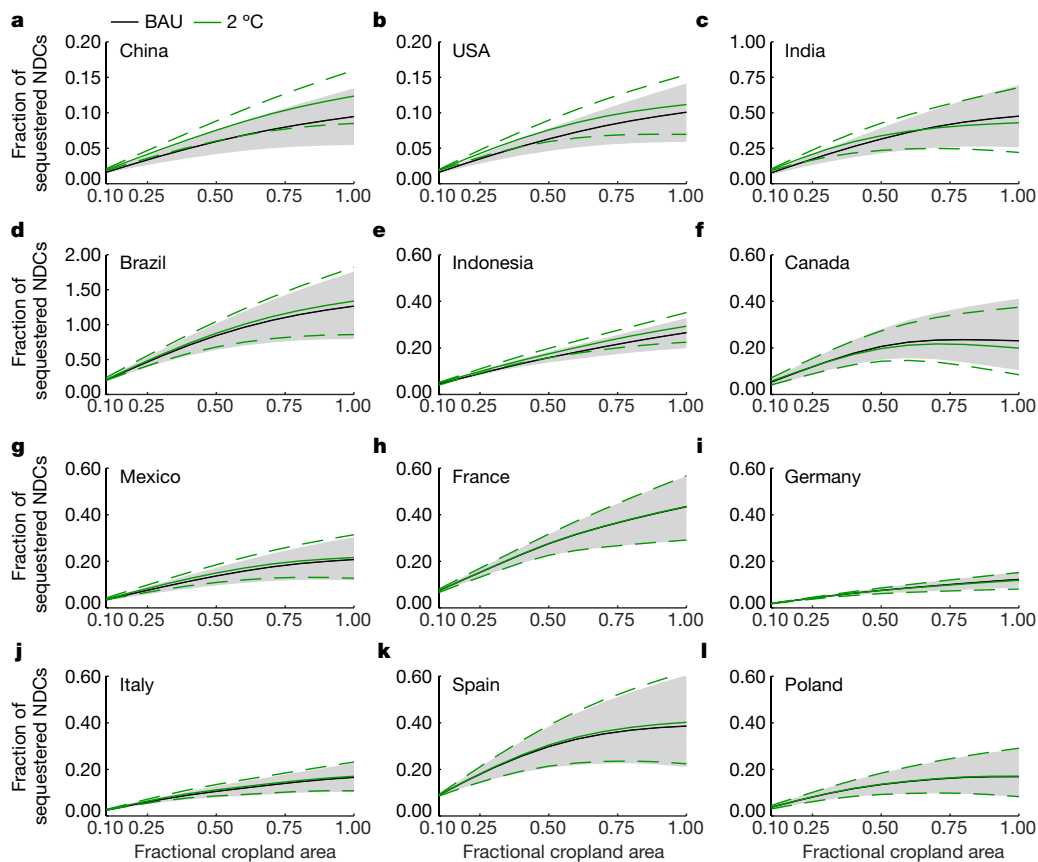
Fig. 2 | Augmentation of pledged CO₂ emissions reduction by ERW. Fraction of 2030 NDC emissions reductions by enhanced weathering for nations with the highest CDR potential worldwide (**a**–**g**) and in Europe (**h**–**l**), as a function of increasing ERW deployment across croplands. Note the *y*-axis scale changes. Results are shown for the BAU energy policy and the 2 °C energy policy scenarios. The grey-shaded area for each nation represents the 90% confidence interval calculated for basalts with relatively slow- versus fast-weathering rates for the BAU scenario; short green dashed lines indicate the 90% confidence limits of the corresponding 2 °C scenario simulations.

emissions from sectors recognized as being difficult to decarbonize, for example, transportation by aviation, shipping and agriculture[1,11].

Costs of CDR via ERW

Cost assessment is needed to evaluate commercial feasibility of ERW and to put a price on climate mitigation actions (Extended Data Fig. 4). Our cost estimates based on current prices (2019 US dollars, throughout) fall within the range of prior ERW assessments (US$75–250 per tonne of CO₂)[21–23] while resolving differences among nations (Fig. 3; Table 1; Supplementary Figs. 16–25; Supplementary Tables 13 and 14). Average costs in USA (US$160–180 per tonne of CO₂), Canada and European nations (US$160–190 per tonne of CO₂) are almost 50% higher than those in China, India, Mexico, Indonesia and Brazil (US$55–120 per tonne of CO₂). The difference largely reflects labour, diesel and electricity costs.

Defined as the cost of CDR and storage, the price of carbon is a proposed economic enabler for bringing CDR strategies to market[11]. Carbon price is forecast by the World Bank[11] to reach US$100–150 per tonne of CO₂ by 2050. Costs per tonne of CO₂ removed by ERW are generally within this projected carbon price range in all nations, but unit costs increase when cropland area exceeds the optimal fraction, because the efficiency of weathering and CDR falls (Fig. 3; Table 1). A carbon price of US$100–150 per tonne of CO₂ would cover most of the ERW costs for the key nations reported here. It would make ERW an economically attractive option for fast-growing nations, such as India, China, Indonesia, Brazil and Mexico, given their estimated CO₂ extraction costs of around US$75–100 per tonne of CO₂ (Fig. 3; Table 1).

Our estimated ERW costs of CDR for nations are comparable to estimates summarized for BECCS (US$100–200 per tonne of CO₂), direct air capture and storage (US$100–300 per tonne of CO₂), and biochar (US$30–US$120 per tonne of CO₂), but higher than estimates for soil

organic carbon sequestration (US$0–10 per tonne of CO₂)[23]. Afforestation/reforestation and practices that increase soil carbon in natural ecosystems, including wetland restoration, have lower estimated costs (<US$100 per tonne of CO₂)[23]. However, these natural carbon sequestration options require assessment for possible indirect unintended positive climate feedbacks.

Per capita metrics help to conceptualize the matter of costs in terms relevant to citizens. Current fossil fuel emissions per person per year[6] are 16.5 t CO₂ (USA), 15.1 t CO₂ (Canada), 7.5 t CO₂ (China), 7.3 t CO₂ (Europe), 2.6 t CO₂ (Brazil), 1.8 t CO₂ (Indonesia) and 1.7 t CO₂ (India). ERW cannot offset all fossil fuel emissions, but using its cost as a guide, the per capita annual cost of achieving zero net emissions, a goal for decarbonization, would be highest for Canada (US$3,004), the USA (US$2,780), China (US$832) and Europe (US$1,288). Costs fall substantially for citizens in Brazil (US$300), Indonesia (US$103) and India (US$135) (Table 1).

At this early stage of research and development, costs are uncertain and ERW is in need of demonstration projects[7,11,12]. Costs are likely to decline as the market expands and technologies develop. This includes emergence of more energy-efficient, low-carbon technologies for rock grinding. Costs may also decline via co-deployment with afforestation/reforestation projects or agroforestry as part of worldwide carbon-offset trading schemes[7]. The net cost of ERW may be lower, given that rock dust is an acceptable fertilizer for organic agriculture, which currently occupies 57.8 million hectares, because it adds economic value by improving soil health, fertility and ecosystem services[35].

Implementation challenges and opportunities

Our analysis of the techno-economic potential for CDR via ERW strengthens the case for evaluating all aspects of practical deployment in developed and developing economies. This includes: meeting rock demand through alternative sources that avoid mining expansion;
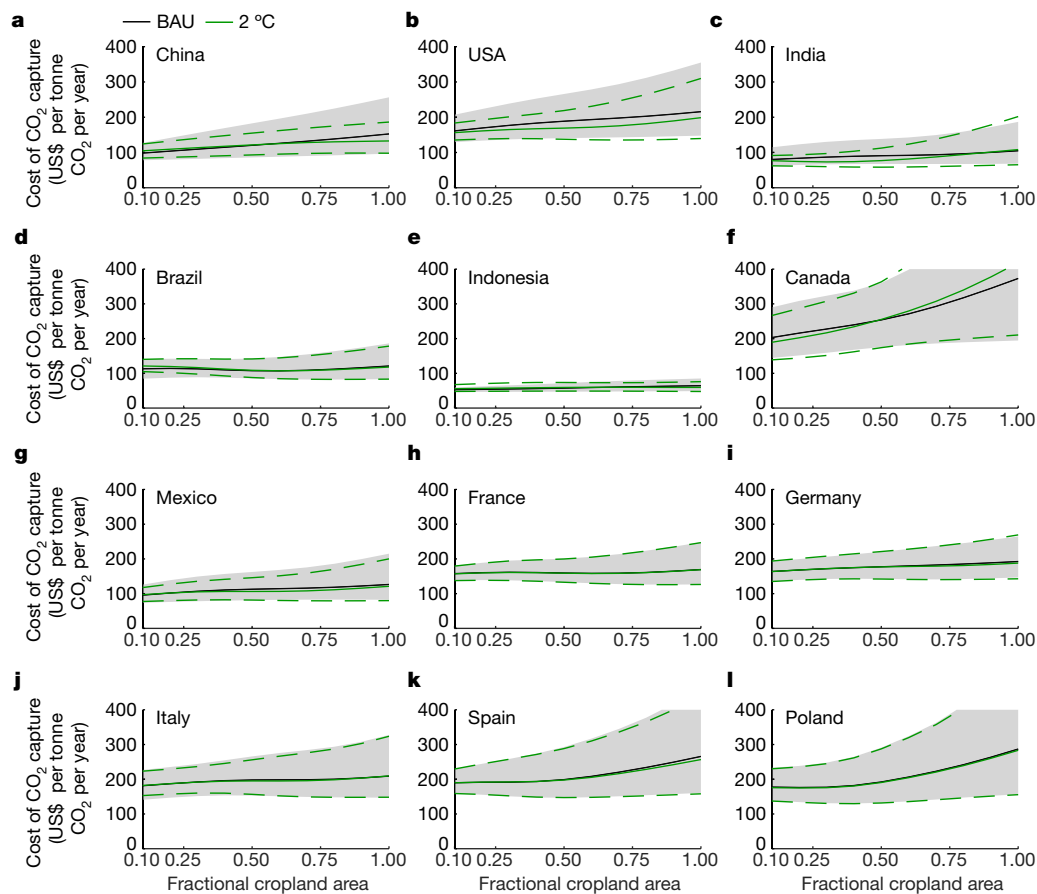
Fig. 3 | Costs of carbon extraction via ERW with croplands. Costs of CO_2 extraction from air by ERW for nations with the highest CDR potential worldwide (**a**–**g**) and in Europe (**h**–**l**), as a function of increasing ERW deployment across croplands. Results are shown for the BAU and the 2 °C energy policy scenarios. The grey-shaded area for each nation represents the 90% confidence interval calculated for basalts with relatively slow- versus fast-weathering rates for the BAU scenario; short green dashed lines indicate the 90% confidence limits of the corresponding 2 °C scenario simulations.

undertaking a more complete economic valuation; and engaging the public to understand social acceptance.

National demand for crushed silicate rock is dependent on the extent of ERW deployment (Extended Data Fig. 5). Within our scenarios, the demand for basalt required for ERW rises with an increasing CDR goal and scales with agricultural land area (Table 1). Safeguarding against substantial increased mining and possible adverse impacts on inhabitants[36] requires exploiting underutilized stockpiles of crushed basalt produced as a by-product of the aggregate industry. Mining generates a continuous, but often discarded, finely powdered silicate by-product that is utilizable for ERW. These materials have been accumulating worldwide for decades and may require no further grinding, thus lowering CO_2 emissions that reduce CDR efficiency (Extended Data Fig. 6)[21–23]. However, national inventories of the location, availability and extent of this resource are required to assess the potential contribution of this resource to CDR via ERW.

Requirement for mining may be further reduced by using artificial silicate by-products from industrial processes[37,38], including calcium-rich silicates produced by iron and steel manufacturing (slags) with a long history of agricultural usage[4,39]. This material is recycled as low-value aggregate (less than about US$5 per tonne), and often stockpiled at production sites or disposed of in landfills, whereas it could become a valuable commodity for CDR. The largest amounts of by-products from the construction and demolition industry are cement, sand and masonry. Following separation from other materials (for example, metals and plastics), the cement comprises relatively 'clean' calcium-rich silicates and may be suitable for application to soils, but this suggestion requires field trials to assess suitability. Cement contributes about 6%

to global CO_2 emissions[6] and ERW may represent a land management option for valuing the by-products of cement and improving the sustainability of this worldwide industry.

We forecast production of artificial calcium-rich cements for construction and by-product slag from steel manufacturing for Brazil, China, India and the USA, to understand their potential role in meeting silicate demand for ERW (Fig. 4). Differences between national production estimates are driven by forecast population increases over the coming century, and per capita consumption trends for the material under the middle-of-the-road Shared Socioeconomic Pathway (see Methods). Bulk silicate production from the construction and demolition sector is modelled to increase substantially in all four nations, with China and India having a combined production by 2060 of about 13 Gt yr^{-1} (Fig. 4). China and India dominate, with above-average per capita cement use compared to the global average, and substantially larger populations than the USA and Brazil[38]. Thus, bulk silicate production of these two nations could meet the demand for ERW with large CDR potential (Table 1). Although chemically similar to basalt, these artificial calcium-rich silicates contain minerals that dissolve several orders of magnitude faster, react rapidly with CO_2 in soils under ambient conditions[40], and are produced in fine particle sizes that facilitate accelerated weathering[41].

Agricultural production could benefit substantially from increased resource use efficiency, reducing consumption of raw materials and recovering mineral nutrients from silicate by-products[32,42,43] and from legacy reserves of silicate rock dust[44]. However, application of any silicate material to agricultural soils requires careful assessment of the risks, including potential release of metals and persistent organic

compounds (Supplementary Table 15). Undertaking ERW practices with these materials addresses a critical need to fertilize soils with silica and other nutrients lost by harvesting that gradually depletes plant-available pools[39]. Intensification of food production across 24 million hectares of productive agricultural land in South Asia and China, for example, is creating acidified, desilicated soils exhausted in plant nutrients (potassium, zinc and available phosphorus) that limit yields[45]. Yet these negative effects may be reversible with ERW treatments such as fertilization of irrigated rice using either natural and/or artificial silicates (for example, recycled steel slags). Such treatments replenish plant available silica pools, increasing yields and soil pH, and decrease the mobility of potentially toxic trace elements (for example, arsenic)[46]. ERW may therefore also have a role in remediation of toxic-metal-contaminated soils and sediments across 20 million hectares of cultivated land in southern China and elsewhere[47].

More broadly, innovative ERW practices via soil amendments with targeted silicate minerals could help to rebuild rapidly deteriorating agricultural soils on which over six billion people depend directly for food[48]. Such practices may complement other approaches to soil improvement, including conservation tillage and nitrogen-fixing cover crops. The current substantial rate of agricultural top-soil depletion requires urgent remedial action, with high economic costs apparent already in China, where degradation of soils supporting wheat, maize and rice production costs an estimated US\$12 billion annually[48]. Targeted amendment of agricultural soils for CDR may have a role in slowing rates of soil loss by up to 45%, with the accelerated weathering of added minerals replacing inorganic nutrients and the resultant formation of clays and mineral organic aggregates increasing the cation exchange capacity and water storage capacity of rebuilt soils[4,20]. The addition of trace amounts of zinc and iron could also improve public health by reversing the effect of rising CO_2 levels on the declining nutritional value of food crops[49].

The feasibility of mobilizing millions of smallholder communities to adopt ERW practices in China and India will depend both on demonstrating that soil improvements can reverse yield declines and on government subsidies. Farming practices adopted for increasing sustainable productivity, for example, have transformed agriculture across 37 million hectares in China, increasing profits by US\$12.2 billion over a decade[50]. With 2.5 billion smallholders farming 60% of the world's arable land, a similar outreach programme could be used throughout Asia, with farmers earning more profits from higher yields while sequestering CO_2. Involving local scientists in conducting research into its effectiveness and safety to build trust and engagement with smallholder farmers is key, alongside involvement with policymakers and stakeholders. This increases the potential to bring smallholders out of extreme poverty and, in the regions with climates suitable for non-irrigated agriculture, restore highly degraded soils not suitable currently for food production.

Realizing the potential of ERW as a biogeochemical approach to sequester CO_2 by altering land management practices will depend on the commitment of farmers and governments, implementation of the right policy frameworks and wider public acceptance. Understanding the balance between positive and negative outcomes, in terms of public acceptance of the inevitable trade-offs between local mining activities versus global sequestered carbon, requires empirical testing with stakeholders and the wider public. Crucially, such testing needs to understand the conditions that society might place upon the development and large-scale deployment of ERW technologies, as part of a wider responsible research and innovation programme[51].

Uncertainties

Our analysis of the techno-economic potential of CDR by ERW is subject to several uncertainties, particularly variation in our baseline application rate and basalt mineralogy. It also identifies priority areas benefitting from more research into ERW under field conditions.
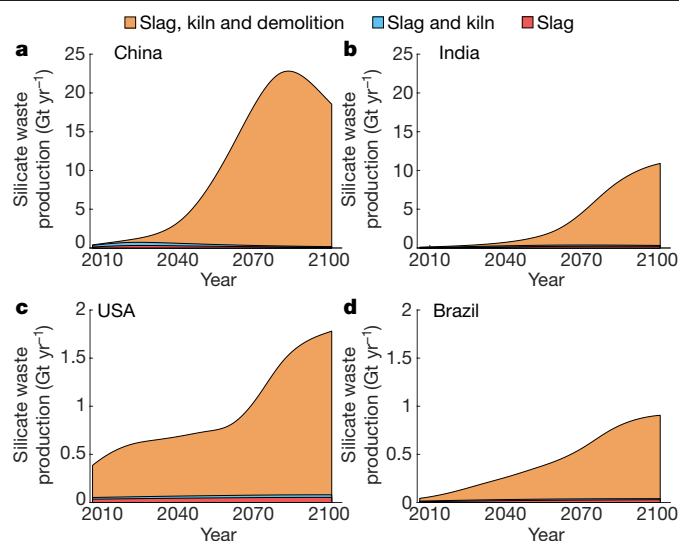
Fig. 4 | Forecast increases in national bulk silicate production over the next century. Simulated future increases in bulk artificial silicate by products (slag, cement, kiln dust and cementitious demolition waste) production during the twenty-first century are given for China (**a**), India (**b**), USA (**c**) and Brazil (**d**), based on the middle-of-the-road Shared Socioeconomic Pathway (Methods).

Extrapolation of laboratory weathering rates to the field scale is a recognized potential source of uncertainty in calculated CDR rates by ERW[2–4,22–24]. We addressed this by Monte Carlo analysis of the fractal dimension accounting for uncertainty in the apparent reacting surface area of grains for ERW conducted at large geographical scales. Together with the chemical affinity effects accounted for in our model, we constrain some of the systematic errors embedded in prior ERW assessments[15–17,21,22].

Surface passivation, a component of chemical inhibition, occurs as weathering proceeds, creating leached layers and relatively stable secondary minerals, which potentially inhibit the mass transfer kinetics of elements from the dissolving surfaces of primary minerals. The current state of knowledge[52] precludes a detailed treatment of the role of surface passivation by formation of amorphous silica-rich surfaces for basalt grains added to agricultural soils. ERW analysis will benefit from future research to improve mechanistic insight and formulation of kinetic equations.

It remains to be determined whether our theoretical analyses of the techno-economic potential for this CDR approach are consistent with findings from long-term field-scale ERW trials. Such trials are urgently required to assess weathering and CDR efficiency of freshly crushed rock grains with highly reactive surfaces added to agricultural soils subject to periodic wet–dry cycles during the growing season[3]. The potential for the trapping of weathered cations on ion exchange surfaces or within secondary minerals other than carbonates, thus delaying or preventing land–ocean transfer, will depend on soil type, climate, hydrological conditions, application rate and management practices. The duration of the carbon sequestration rate, and the possibility of CO_2 sink saturation with ERW on croplands, are both poorly constrained by data, as for other land-based CDR strategies[11,23]. Other areas for further research include: the quantification of biogeochemical transformations of carbon and nitrogen associated with organic and inorganic fertilization practices; atmospheric deposition; and the role of rhizosphere biology.

Conclusions

The techno-economic assessment of ERW's potential to contribute large-scale CDR requires further integration of nation-by-nation quantitative analysis, together with large-scale pilot demonstrations

Article

supported by fundamental process studies and public engagement. Our analysis identifies the engineering challenges if ERW were to be scaled up to help meet ambitious CDR goals as part of a wider portfolio of options[1,7,11,12]. ERW estimated costs are comparable to (and generally lower than) current estimates for the intensive CDR technologies—BECCS and direct air capture—and have potential ancillary benefits through limiting coastal zone acidification and improving food and soil security. Nations that may have large ERW potential, including China, the USA and India, are all vulnerable to climate change and resultant sea-level rise[34]. Their high risks of economic damage[53] and social disruption should provide the impetus for creative co-design of agricultural and climate policies. Success requires incentives and regulatory frameworks that overcome social and political inertia. Silicate demand of nations must also be met in a way that facilitates social acceptance[51,54] and preservation of biodiversity[4,20].

Deployment of any CDR strategy is inhibited by the concern that it may erode society's perception of the climate threat and the urgency of mitigation measures[54]. However, the ancillary benefits of ERW may aid its early use by creating 'demand pull', and relieve such concern. Innovative 'climate-smart' farming practices can be designed with ERW to draw down CO_2 and other greenhouse gases while recycling nutrients, aiding soil water storage, and supporting crop production[4,18,20]. Such practices can help to restore deteriorating topsoils that underpin food security for billions of people while maximizing the societal co-benefits needed to incentivize deployment[20]. Financial, industrial and policy road-mapping that links the possibility to reliably set and achieve short-term and long-term goals is needed, including a broader analysis of risks[23] and co-benefits[2–4,18,20], to determine the part that ERW might play in climate risk mitigation.

Online content

Any methods, additional references, Nature Research reporting summaries, source data, extended data, supplementary information, acknowledgements, peer review information; details of author contributions and competing interests; and statements of data and code availability are available at https://doi.org/10.1038/s41586-020-2448-9.

1. Intergovernmental Panel on Climate Change (IPCC). *Global Warming Of 1.5 °C. An IPCC Special Report on the Impacts of Global Warming of 1.5 °C Above Pre-Industrial Levels and Related Global Greenhouse Gas Emission Pathways* (World Meteorological Organization, 2018).
2. Kantola, I. B. et al. Potential of global croplands and bioenergy crops for climate change mitigation through deployment for enhanced weathering. *Biol. Lett.* **13**, 20160714 (2017).
3. Zhang, G., Kang, J., Wang, T. & Zhu, C. Review and outlook for agromineral research in agriculture and climate change mitigation. *Soil Res.* **56**, 113–122 (2018).
4. Beerling, D. J. et al. Farming with crops and rocks to address global climate, food and soil security. *Nat. Plants* **4**, 138–147 (2018).
5. Mercure, J.-F. et al. Macroeconomic impact of stranded fossil fuel assets. *Nat. Clim. Chang.* **8**, 588–593 (2018).
6. Le Quéré, C. et al. Global carbon budget 2018. *Earth Syst. Sci. Data* **10**, 2141–2194 (2018).
7. United Nations Environment Programme *The Emissions Gap Report 2018* (United Nations Environment Programme, 2018).
8. Hagedorn, G. et al. Concerns of young protesters are justified. *Science* **364**, 139–140 (2019).
9. Hansen, J. et al. Young people's burden: requirement of negative CO_2 emissions. *Earth Syst. Dyn* **8**, 577–616 (2017).
10. Rockström, J. et al. A roadmap for rapid decarbonisation. *Science* **355**, 1269–1271 (2017).
11. *The Royal Society Greenhouse Gas Removal Technologies* (The Royal Society, 2018).
12. Pacala, S. et al. *Negative Emissions Technologies And Reliable Sequestration* (National Academy of Sciences, 2018).
13. Seifritz, W. CO_2 disposal by means of silicates. *Nature* **345**, 486 (1990).
14. Schuiling, R. D. & Krijgsman, P. Enhanced weathering: an effective and cheap tool to sequester CO_2. *Clim. Change* **74**, 349–354 (2006).
15. Kohler, P., Hartmann, J. & Wolf-Gladrow, D. A. Geoengineering potential of artificially enhanced silicate weathering of olivine. *Proc. Natl Acad. Sci. USA* **107**, 20228–20233 (2010).
16. Hartmann, J. et al. Enhanced chemical weathering as a geoengineering strategy to reduce atmospheric carbon dioxide, supply nutrients, and mitigate ocean acidification. *Rev. Geophys.* **51**, 113–149 (2013).
17. Taylor, L. L. et al. Enhanced weathering strategies for stabilizing climate and averting ocean acidification. *Nat. Clim. Chang.* **6**, 402–406 (2016).
18. Kelland, M. E. et al. Increased yield and CO_2 sequestration potential with the C_4 cereal crop *Sorghum bicolor* cultivated in basaltic rock dust amended agricultural soil. *Glob. Change Biol.* **26**, 3658–3676 (2020).
19. Renforth, P. & Henderson, G. Assessing ocean alkalinity for carbon sequestration. *Rev. Geophys.* **55**, 636–674 (2017).
20. Smith, P. et al. Land-based options for greenhouse gas removal and their impacts on ecosystem services and the sustainable development goals. *Annu. Rev. Environ. Res.* **44**, 255–286 (2019).
21. Renforth, P. The potential of enhanced weathering in the UK. *Int. J. Greenhouse Gas Control* **10**, 229–243 (2012).
22. Strefler, J. et al. Potential and costs of carbon dioxide removal by enhanced weathering of rocks. *Environ. Res. Lett.* **13**, 034010 (2018).
23. Fuss, S. et al. Negative emissions—Part 2: Costs, potentials and side effects. *Environ. Res. Lett.* **13**, 063002 (2018).
24. Baik, E. et al. Geospatial analysis of near-term potential for carbon-negative bioenergy in the United States. *Proc. Natl Acad. Sci. USA* **115**, 3290–3295 (2018).
25. Heck, V., Gerten, D., Lucht, W. & Popp, A. Biomass-based negative emissions difficult to reconcile with planetary boundaries. *Nat. Clim. Chang.* **8**, 151–155 (2018).
26. Amann, T. & Hartmann, J. Ideas and perspectives: synergies from co-deployment of negative emissions technologies. *Biogeosciences* **16**, 2949–2960 (2019).
27. Mayer, A. et al. The potential of agricultural land management to contribute to lower global surface temperature. *Sci. Adv.* **4**, eaaq0932 (2018).
28. Groffman, P. M. et al. Calcium additions and microbial nitrogen cycle processes in a northern hardwood forest. *Ecosystems* **9**, 1289–1305 (2006).
29. Dietzen, C., Harrison, R. & Michelsen-Correa, S. Effectiveness of enhanced mineral weathering as a carbon sequestration tool and alternative to agricultural lime: an incubation experiment. *Int. J. Greenhouse Gas Control* **74**, 251–258 (2018).
30. Smith, P., Haszeldine, R. S. & Smith, S. M. Preliminary assessment of the potential for, and limitations to, terrestrial negative emissions technologies in the UK. *Environ. Sci. Process. Impacts* **18**, 1400–1405 (2016).
31. DeLucia, E., Kantola, I., Blanc-Betes, E., Bernacchi, C. & Beerling, D. J. Basalt application for carbon sequestration reduces nitrous oxide fluxes from cropland. *Geophys. Res. Abstr.* **21**, EGU2019–EGU4500 (2019).
32. Das, S. et al. Cropping with slag to address soil, environment, and food security. *Front. Microbiol.* **10**, 1320 (2019).
33. Rogelj, J. et al. Paris Agreement climate proposals need a boost to keep warming well below 2 °C. *Nature* **534**, 631–639 (2016).
34. Clark, P. U. et al. Consequences of twenty-first-century policy for multi-millennial climate and sea-level change. *Nat. Clim. Chang.* **6**, 360–369 (2016).
35. Crowder, D. W. & Reganold, J. P. Financial competitiveness of organic agriculture on a global scale. *Proc. Natl Acad. Sci. USA* **112**, 7611–7616 (2015).
36. Bebbington, A. J. & Bury, J. T. Institutional challenges for mining and sustainability in Peru. *Proc. Natl Acad. Sci. USA* **106**, 17296–17301 (2009).
37. Renforth, P. et al. Silicate production and availability for mineral carbonation. *Environ. Sci. Technol.* **45**, 2035–2041 (2011).
38. Renforth, P. The negative emission potential of alkaline materials. *Nat. Commun.* **10**, 1401 (2019).
39. Tubana, B. S., Babu, T. & Datnoff, L. E. A review of silicon in soils and plants and its role in US agriculture: history and future perspectives. *Soil Sci.* **181**, 393–411 (2016).
40. Washbourne, C.-L. et al. Rapid removal of atmospheric CO_2 in urban soils. *Environ. Sci. Technol.* **49**, 5434–5440 (2015).
41. Lekakh, S. N. et al. Kinetics of aqueous leaching and carbonization of steelmaking slag. *Metallurg. Mater. Trans. B* **39**, 125–134 (2008).
42. Haynes, R. J., Belyaeva, O. N. & Kingston, G. Evaluation of industrial waste sources of fertilizer silicon using chemical extractions and plant uptake. *J. Plant Nutr. Soil Sci.* **176**, 238–248 (2013).
43. Rodd, A. V. et al. Surface application of cement kiln dust and lime to forage land: effect on forage yield, tissue concentration and accumulation of nutrients. *Can. J. Soil Sci.* **90**, 201–213 (2010).
44. Ramos, C.G. et al. Evaluation of soil re-mineralizer from by-product of volcanic rock mining: experimental proof using black oats and maize crops. *Nat. Res. Res.* 10.1007/s11053–019–09529-x (2019).
45. Savant, N. K., Datnoff, L. E. & Snyder, G. H. Depletion of plant-available silicon in soils: a possible cause of declining rice yields. *Commun. Soil Sci. Plant Anal.* **28**, 1245–1252 (1997).
46. Ning, D. et al. Impacts of steel-slag-based fertilizer on soil acidity and silicon availability and metals-immobilization in a paddy soil. *PLoS One* **11**, e0168163 (2016).
47. Chen, J. Rapid urbanization in China: a real challenge to soil protection and food security. *Catena* **69**, 1–15 (2007).
48. United Nations *Global Land Outlook* 1st edn (United Nations Convention to Combat Desertification, 2017).
49. Smith, M. R. & Myers, S. S. Impact of anthropogenic CO_2 emissions on global human nutrition. *Nat. Clim. Chang.* **8**, 834–839 (2018).
50. Cui, Z. et al. Pursuing sustainable productivity with millions of smallholder farmers. *Nature* **555**, 363–366 (2018).
51. Pidgeon, N. F. & Spence, E. Perceptions of enhanced weathering as a biological negative emissions option. *Biol. Lett.* **13**, 20170024 (2017).
52. Daval, D., Calvarusa, C., Guyut, F. & Turpault, M.-P. Time-dependent feldspar dissolution rates resulting from surface passivation: experimental evidence and geochemical implications. *Earth Planet. Sci. Lett.* **498**, 226–236 (2018).
53. Ricke, K., Drout, L., Caldeira, K. & Tavoni, M. Country-level social cost of carbon. *Nat. Clim. Chang.* **8**, 895–900 (2018).
54. Cox, E., Pidgeon, N. F., Spence, E. M. & Thomas, G. Blurred lines: the ethics and policy of greenhouse gas removal at scale. *Front. Environ. Sci.* https://doi.org/10.3389/fenvs.2018.00038 (2018).

Methods

CDR simulation framework

Our analysis is based on a one-dimensional vertical reactive transport model for rock weathering with steady-state flow[55,56], and a source term representing rock grain dissolution within the soil profile (Supplementary Methods). The model accounts for changing dissolution rates with soil depth and time as grains dissolve, and chemical inhibition of dissolution as pore fluids approach equilibrium with respect to the reacting basaltic mineral phases, and the formation of pedogenic calcium carbonate mineral in equilibrium with pore fluids. Simulations consider basalts exhibiting relatively slow- versus fast-dissolution rates due to differing mineralogy (Supplementary Tables 1–3). Basaltic minerals undergo dissolution at different rates, with some minerals continuing to undergo dissolution and to capture CO_2 after the first year of application. Thus calculating representative annual CDR rates requires computing average rates derived from repeated basaltic rock dust applications (Extended Data Fig. 7).

Transport equation. The calculated state variable in the transport equation is the dissolved molar equivalents of elements released by stoichiometric dissolution of mineral i, in units of moles per litre. ϕ is volumetric water content, C_i is dissolved concentration (moles per litre) of mineral i transferred to solution, t is time (years), q is vertical water flux (metres per year), z is distance along vertical flow path (metres), R_i is the weathering rate of basalt mineral i (moles per litre of bulk soil per year) and $C_{eq,i}$ is the solution concentration of weathering product at equilibrium with the mineral phase i (equation (1)):

$$\phi \frac{\partial C_i}{\partial t} = -q \frac{\partial C_i}{\partial z} + R_i \left(1 - \frac{C_i}{C_{eq,i}} \right) \qquad (1)$$

Mineral mass balance. The change in mass of basalt mineral i, B_i, is defined by the rate of stoichiometric mass transfer of the elements in mineral i to solution. Equation (2) is required because we are considering a finite mass of weathering rock, which over time can react to completion, as opposed to in situ weathering of the lithosphere, for example, when considering weathering and geomorphology[56].

$$\frac{\partial B_i}{\partial t} = -R_i \left(1 - \frac{C_i}{C_{eq,i}} \right) \qquad (2)$$

Removal of weathering products. The total mass balance over time for basalt mineral weathering allows calculation of the products transported from the soil profile. The total mass of weathering basalt is defined as follows, where m is the total number of weathering minerals in the rock, t_f is the duration of weathering (years) and L is the total depth of the soil profile (metres).

$$\text{Total mass of weathered basalt} = \sum_{i=1}^{m} \phi \int_{z=0}^{L} C_i(t,z)\,dz + q \int_{t=0}^{t_f} C_i(t,L)\,dt \qquad (3)$$

We define q as the net annual sum of water gained through precipitation[57] and irrigation[58], minus crop evapotranspiration[59], as calculated with high-spatial-resolution gridded datasets of the contemporary climate in this initial analysis, given the uncertainties in infiltration and irrigation patterns at equivalent high spatial resolution for 2050 (Extended Data Figs. 8, 9; Supplementary Table 14).

Rate law. We modelled application of a crushed fast- or slow-weathering basalt, with specified mineral weight fractions and physico-chemical characteristics (Supplementary Tables 1–3). Rates of basalt grain weathering define the source term for weathering products and are calculated as a function of soil pH, soil temperature, soil hydrology and

crop net primary productivity (NPP) using the linear transition state theory rate law[60–62]. Plant-enhanced basalt weathering is modelled empirically for annual and woody crops with power functions fitted to data (Supplementary Fig. 4; Supplementary Table 4). These functions represent the effects of a range of rhizosphere processes that accelerate the physical breakdown and chemical dissolution of minerals, including the activities of nutrient-scavenging mycorrhizal fungi that physically disrupt and chemically etch mineral surfaces, and bio-production of low-molecular-weight organic compounds and chelating agents[63,64].

Soil pH of each grid cell is dynamically calculated from the alkalinity mass and flux balance for an adaptive time-step, controlled by mineral dissolution rates, following initialization with a topsoil (0–15 cm) pH value based on field data from global soil databases (Supplementary Table 14); soil pH buffering capacity is accounted for with an empirical buffer function[65] relating soil pH to alkalinity. The soil p_{CO_2} depth profile of a grid cell is generated with the standard gas diffusion equation[66], scaled by crop NPP × 1.5 to account for combined autotrophic and heterotrophic respiration[67]. The alkalinity balance considers net acidity input during crop growth for biomass cations removed from the field[68], and secondary mineral precipitation of calcite[18].

Model advances

We incorporate three further relevant advances into the above one-dimensional vertical transport model with steady-state flow. First, we provide a numerical basis for calculating weathering rates using log-normal particle size distributions of basalt grains produced by mechanical crushing and grinding for soil amendment[22,69,70]. This conceptualization improves on the simplified case of a single mean particle diameter, previously used in ERW calculations[16–18,22,23]. Second, we apply the fractal dimension for surface roughness to relate reacting surface area to basalt mass across physical scales of weathering from the laboratory (in which the weathering kinetic parameter values are empirically determined) to the field (where model results reflect CDR operations)[71]. The fractal dimension effectively provides a means of consolidating measurements taken at different scales, and accounts for uncertainties in grain topography and porosity[72] that affect mass transfer rates from rock grains to flowing soil water. Finally, we calculate mean rates of rock dust weathering and CDR following annual applications by tracking cohorts of particles applied over a 10-year time horizon and their mineral composition (Extended Data Fig. 7).

Baseline simulations

Using this modelling framework, we analysed a baseline application rate of 40 tonnes per hectare per year (equivalent to a <2 mm layer of rock powder distributed over the croplands), which falls within the range of basalt amendments shown to improve crop production in field trials[4]. Net CDR is defined as the difference between CO_2 capture by ERW as dissolved inorganic carbon and soil (pedogenic) carbonate and the sum of CO_2 emissions for logistical operations. Carbon emissions per unit mass of ground rock depend on particle size (Extended Data Fig. 10), the CO_2 emissions per kilowatt hour of electricity generated from component energy sources (fossil fuels, nuclear and renewables), as well as the carbon costs of sourcing and transporting the silicate materials. Rock grinding to reduce particle size and maximize CDR is the primary energy-consuming operation in ERW[22,23,73].

Assessment of basalt transport from source regions to croplands is based on road and rail network analyses to calculate distances, costs and carbon emissions for each scenario (Supplementary Methods section 2.3). Our approach improves on prior analyses, which assumed a fixed radius between rock dust source and site of application[73]. We go beyond global cost estimates[23] by using national fuel (diesel), labour and infrastructure costs to undertake logistical operations, and the price of energy inputs to grind rocks. Our analysis thus represents the first techno-economic assessment in which detailed ERW carbon

Article

and economic costs vary within and between nations and account for socio-technical uncertainties in energy production.
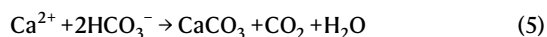
CDR

We calculate CDR by ERW of crushed basalt applied to soils via two pathways: (1) the transfer of weathered base cations (Ca^{2+}, Mg^{2+}, Na^+ and K^+) from soil drainage waters to surface waters that are charge-balanced by the formation of HCO_3^- ions and transported to the ocean (equation (4)), and (2) formation of pedogenic carbonates (equation (5)).

Pathway 1 for calcium ions:

$$CaSiO_3 + 2CO_2 + 3H_2O \rightarrow Ca^{2+} + 2HCO_3^- + H_4SiO_4 \qquad (4)$$
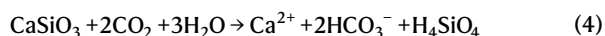
Pathway 2 for calcium carbonate formation:

$$Ca^{2+} + 2HCO_3^- \rightarrow CaCO_3 + CO_2 + H_2O \qquad (5)$$

Monovalent and divalent base cations are released from basaltic minerals by dissolution based on stoichiometry (Supplementary Table 2). CDR, via pathway 1, potentially sequesters two moles of CO_2 from the atmosphere per mole of divalent cation. However, ocean carbonate chemistry reduces the efficiency of CDR (η) to an extent depending on ocean temperature, salinity and the surface ocean dissolved CO_2 concentration. We calculate η for average ocean temperature (17 °C), salinity (35%) and a Representative Concentration Pathway (RCP) 8.5 simulation for 2050 (the worst-case scenario) for dissolved p_{CO_2} of 600 µatm, giving $\eta = 0.86$, that is, 0.86 moles of CDR per mole of monovalent cation and 1.72 moles of CO_2 removed per mole of divalent cation added to the oceans[20]. For pathway 1, the efficiency of CDR = $\eta \times \sum$ (moles of monovalent cations) + $2\eta \times \sum$ (moles of divalent cations).

CDR via pathway 2 can occur if dissolved inorganic carbon derived from atmospheric CO_2 precipitates as pedogenic carbonate, and sequesters 1 mole of CO_2 per mole of Ca^{2+} instead of 1.72 moles of CO_2 via pathway 1 and is therefore less efficient. Thus for any given grid cell, we compute CDR by ERW as the alkalinity flux in soil drainage and pedogenic calcite precipitation. Possible CO_2 degassing due to changes in surface water chemistry during transport in large river systems[74] is not considered.

Cost assessment modelling

An overview of the environmental costs model and its linkages with the performance model is presented in Extended Data Fig. 4. We include contributions to total cost of (1) mining, (2) processing[75,76], (3) distribution and transport and (4) spreading on agricultural land. We considered how the cost of energy and the carbon emissions varied with grinding to different particle size distributions (Extended Data Fig. 10). Grinding to finer particles requires greater energy and results in higher carbon emissions. We defined the particle size distribution by the p80 value; p80 is defined as 80% of the particles having a diameter less than or equal to a specified particle size. We calculated the optimized p80 that results in maximum net CDR for each grid cell and this was conducted for different fractions of a country's crop area (0.1 to 1.0 at 0.1 increments), ordered according to weathering potential. For a given p80 value, we calculate the weathering rate for each grid cell, sort them in descending order and find the grid cells that comprise the cumulative fraction of total land for each incremental increase in land area.

Optimization is conducted by country for each of the two types of basalt and their log-normal particle size distributions (Supplementary Tables 1–3). Country-specific electricity production and the forecast fractional contributions to electricity production by different energy sources (coal, natural gas, oil, solar photovoltaics, concentrated solar power, hydropower, wind, marine) for 2050 are based on BAU, that is, currently implemented energy policies, and energy projections consistent with a 2 °C warming scenario (Extended Data Fig. 9)[5]. National

CO_2 emissions for electricity generation consistent with both scenarios were based on results reported in ref. [5] (Supplementary Tables 6–9). Industrialized nations (for example, Canada) consume up to about 2% of their total energy production on rock comminution (crushing and grinding) processes[77]. We assume a future maximum upper limit of 3% energy consumption for all nations, based on the rationale that current rates for developed nations grow from around 2% today in line with national projected energy production[5] in 2050 (Extended Data Fig. 2).

Distribution costs and emissions were calculated by performing spatial analysis with ArcGIS (http://www.arcgis.com) software. Basalt rock sources were identified from the GLiM rock database[78], excluding those in protected areas[79]. We then performed a global transport (rail and road) network analysis by modelling a logistic ERW supply by creating an origin–destination cost matrix using GIS[80,81]. For larger datasets, the origin–destination cost matrix searches and measures the least-cost paths along the network from multiple origins to multiple destinations to identify the most cost-effective or shortest route between a source and destination. Transport analyses used the lowest-emission option between rail and road network to calculate distribution costs and CO_2 emissions (Supplementary Tables 10–12). Freight-rail emissions were obtained from 2050 projections of reduced carbon emissions following improvements in energy efficiency[82]. Rail CO_2 emissions were the same for both the BAU and 2 °C scenarios. For road transport, we considered estimated energy consumption of currently or soon-to-be available heavy electric trucks 1.38 (kWh km^{-1})[83] and projected carbon emissions in the electricity sector of each country for BAU or the 2 °C scenario[5].

Forecasting bulk silicate waste production

We developed a model that relates global per capita material production (for cement) or consumption (steel) P to per capita gross world product (GWP)[84,85] through historical global data using nonlinear least squares (equation (6)):

$$P = a e^{-b/GWP} \qquad (6)$$

where a and b are regression constants. The derived saturation value, a, was used in a further regression through national data normalized to 2014 production and GDP (equation (7).

$$P = P_{ref} \times [1 + (m + r) \times \Delta GDP] \times e^{a \times (1 - e^{-m \times \Delta GDP}) - (m \times \Delta GDP)} \qquad (7)$$

where P_{ref} is the global per capita consumption in a given reference year (2014), ΔGDP is the deviation of the per capita gross domestic product from the reference year, and m and r are regression constants. These results were used together with averaged projections of future GDP (Supplementary Table 14) from the 'middle-of-the-road' Shared Socio-economic Pathway (SSP2) to derive nationally resolved projections of future per capita consumption/production[85]. SSP2 potentially represents the largest material production pathway, as other SSPs forecast lower consumption or economic growth producing 30% to 50% less material globally. We have not considered the penetration of recycling into steel production beyond its current rate. Cement and cement kiln dust have no capacity to be recycled as cement. The total production/consumption at a given time, $T(t)$, was calculated by multiplying the population, Pop(t), by production or consumption (P). We assume that 115 kg of cement kiln dust is produced as a by-product in kilns for every tonne of clinker, and have modelled the production of demolition waste following an average 50-year service life (normally distributed with a standard deviation of 10 years)[86]. The ratio of pig iron to steel production (0.72) was obtained using linear regression of 1960–2014 data, negating the need to explicitly model pig iron displacement from scrap recycling, and assuming that the scrap ratio remains unchanged. All steel and blast furnace slag was considered available for reaction

with CO_2. Between 2006 and 2014, 185 kg of blast furnace slag and 117 kg of steel slag was produced for every tonne of crude steel[87].

Data availability

Datasets on global crop production and yield are available at http://www.earthstat.org/, accessed on 18 December 2019. Datasets on global crop irrigation are available at https://zenodo.org/record/1209296, accessed on 18 December 2019. Datasets on global precipitation are available at http://www.climatologylab.org/terraclimate.html, accessed on 18 December 2019. Datasets on global soil surface pH are available at https://daac.ornl.gov/SOILS/guides/HWSD.html, accessed on 18 December /2019. Datasets on global soil temperature are available at https://esgf-node.llnl.gov/search/cmip5/, accessed on 18 December 2019. Datasets on diesel prices are available at https://data.worldbank.org/indicator/EP.PMP.DESL.CD. Datasets on mining costs are available at http://www.infomine.com/. Datasets on gross national income per capita are available at https://data.worldbank.org/indicator/ny.gnp.pcap.pp.cd. Datasets for projections of future GDP linked to Shared Socioeconomic Pathways are available at https://tntcat.iiasa.ac.at/SspDb. Source data are provided with this paper.

Code availability

The Matlab codes developed for this study belong to the Leverhulme Centre for Climate Change Mitigation. The authors will make them available upon reasonable request.

55. Berner, R. A. Rate control of mineral dissolution under Earth surface conditions. *Am. J. Sci.* **278**, 1235–1252 (1978).
56. Maher, K. The dependence of chemical weathering rates on fluid residence time. *Earth Planet. Sci. Lett.* **294**, 101–110 (2010).
57. Abatzoglou, J. T., Dobrowski, S. Z., Parks, S. A. & Hegewisch, K. C. TerraClimate, a high-resolution global dataset of monthly climate and climatic water balance from 1958-2015. *Sci. Data* **5**, 170191 (2018).
58. Huang, Z. W. et al. Reconstruction of global gridded monthly sectoral water withdrawals for 1971-2010 and analysis of their spatiotemporal patterns. *Hydrol. Earth Syst. Sci.* **22**, 2117–2133 (2018).
59. Siebert, S. & Doll, P. Quantifying blue and green virtual water contents in global crop production as well as potential production losses without irrigation. *J. Hydrol.* **384**, 198–217 (2010).
60. Aagaard, P. & Helgeson, H. C. Thermodynamic and kinetic constraints on reaction-rates among minerals and aqueous-solutions. 1. *Theoretical considerations. Am. J. Sci.* **282**, 237–285 (1982).
61. Lasaga, A. C. Chemical-kinetics of water-rock interactions. *J. Geophys. Res.* **89**, 4009–4025 (1984).
62. Brantley, S. L., Kubicki, J. D. & White, A. F. *Kinetics of Water–Rock Interaction* (Springer, 2008).
63. Harley, A. D. & Gilkes, R. J. Factors influencing the release of plant nutrient elements from silicate rock powders: a geochemical overview. *Nutr. Cycl. Agroecosyst.* **56**, 11–36 (2000).
64. Taylor, L. L. et al. Biological evolution and the long-term carbon cycle: integrating mycorrhizal evolution and function into the current paradigm. *Geobiology* **7**, 171–191 (2009).
65. Nelson, P. N. & Su, N. Soil pH buffering capacity: a descriptive function and its application to some acidic tropical soils. *Aust. J. Soil Sci.* **48**, 201–207 (2010).
66. Cerling, T. Carbon dioxide in the atmosphere: evidence from Cenozoic and Mesozoic paleosols. *Am. J. Sci.* **291**, 377–400 (1991).
67. Taylor, L., Banwart, S. A., Leake, J. R. & Beerling, D. J. Modelling the evolutionary rise of ectomycorrhizal on sub-surface weathering environments and the geochemical carbon cycle. *Am. J. Sci.* **311**, 369–403 (2011).
68. Banwart, S. A., Berg, A. & Beerling, D. J. Process-based modeling of silicate mineral weathering responses to increasing atmospheric CO_2 and climate change. *Glob. Biogeochem. Cycles* **23**, GB4013 (2009).
69. Petavratzi, E., Kingman, S. & Lowndes, I. Particulates from mining operations: a review of sources, effects and regulations. *Miner. Eng.* **18**, 1183–1199 (2005).
70. Cepuritis, R., Garboczi, E. J., Ferraris, C. F., Jacobsen, S. & Sorensen, B. E. Measurement of particle size distribution and specific surface area for crushed concrete aggregate fines. *Adv. Powder Technol.* **28**, 706–720 (2017).
71. Navarre-Sitchler, A. & Brantley, S. Basalt weathering across scales. *Earth Planet. Sci. Lett.* **261**, 321–334 (2007).
72. Brantley, S. L. & Mellott, N. P. Surface area and porosity of primary silicate minerals. *Am. Mineral.* **85**, 1767–1783 (2000).
73. Moosdorf, N., Renforth, P. & Hartmann, J. Carbon dioxide efficiency of terrestrial weathering. *Environ. Sci. Technol.* **48**, 4809–4816 (2014).
74. Salisbury, J. E. et al. Seasonal observations of surface waters in two Gulf of Maine estuary-plume systems: relationships between watershed attributes, optical measurements and surface p_{CO_2}. *Estuar. Coast. Shelf Sci.* **77**, 245–252 (2008).
75. Darling, P. & Society for Mining, Metallurgy and Exploration (U.S.). *SME Mining Engineering Handbook* 3rd edn (Society for Mining, Metallurgy and Exploration, 2011).
76. *InfoMine, Mining Cost Service* http://www.infomine.com/ (Infomine, 2009).
77. Tromans, D. Mineral comminution: energy efficiency considerations. *Min. Eng.* **21**, 613–620 (2008).
78. Hartmann, J. & Moosdorf, N. The new global lithological map database GLiM: a representation of rock properties at the Earth surface. *Geochem. Geophys. Geosyst.* **13**, Q12004 (2012).
79. Protected Planet: The World Database on Protected Areas (WDPA)/The Global Database on Protected Areas Management Effectiveness (GD-PAME) https://www.protectedplanet.net/ (UNEP-WCMC and IUCN, 2018).
80. ROTARU, A. S. et al. Modelling a logistic problem by creating an origin-destination cost matrix using GIS technology. *Bull. UASVM Horticulture* **71**, https://doi.org/10.15835/buasvmcn-hort:9697 (2014).
81. Osorio, C. Dynamic origin-destination matrix calibration for large-scale network simulators. *Transport. Res. C* **98**, 186–206 (2019).
82. *International Energy Agency The Future of Rail, Opportunities for Energy and the Environment* (International Energy Agency, 2019).
83. Liimatainen, H., van Vliet, O. & Aplyn, D. The potential of electric trucks—an international commodity-level analysis. *Appl. Energy* **236**, 804–814 (2019).
84. *GDP (current US$)* https://data.worldbank.org/indicator/NY.GDP.MKTP.CD (The World Bank, 2016).
85. Bauer, N. et al. Shared socio-economic pathways of the energy sector – quantifying the narratives. *Glob. Environ. Change* **42**, 316–330 (2017).
86. Xi, F. et al. Substantial global carbon uptake by cement carbonation. *Nat. Geosci.* **9**, 880–883 (2016).
87. U.S. Geological Survey. *Mineral Commodity Summaries 2006* (US Geological Survey, 2006).

Author contributions D.J.B., E.P.K., M.R.L., P.W., S.Q. and S.A.B. designed the study, E.P.K. and M.R.L. undertook model development and coding, with input from P.W., S.A.B., S.Q. and D.J.B. E.P.K. undertook data analysis and synthesis, R.M.E. and L.K. undertook the GIS transport analyses, P.R. did the silicate production modelling, and N.F.P. wrote sections on public perception. J.-F.M., H.P., N.R.E. and P.B.H. provided data on national energy production and sources, and CO_2 emissions for both scenarios. M.G.A., R.H.J., C.R.P., M.K., B.S. and I.A.J. all provided input on sections and addition of appropriate references specific to their area of expertise. D.J.B. and S.A.B. wrote the manuscript, with input from J.H.
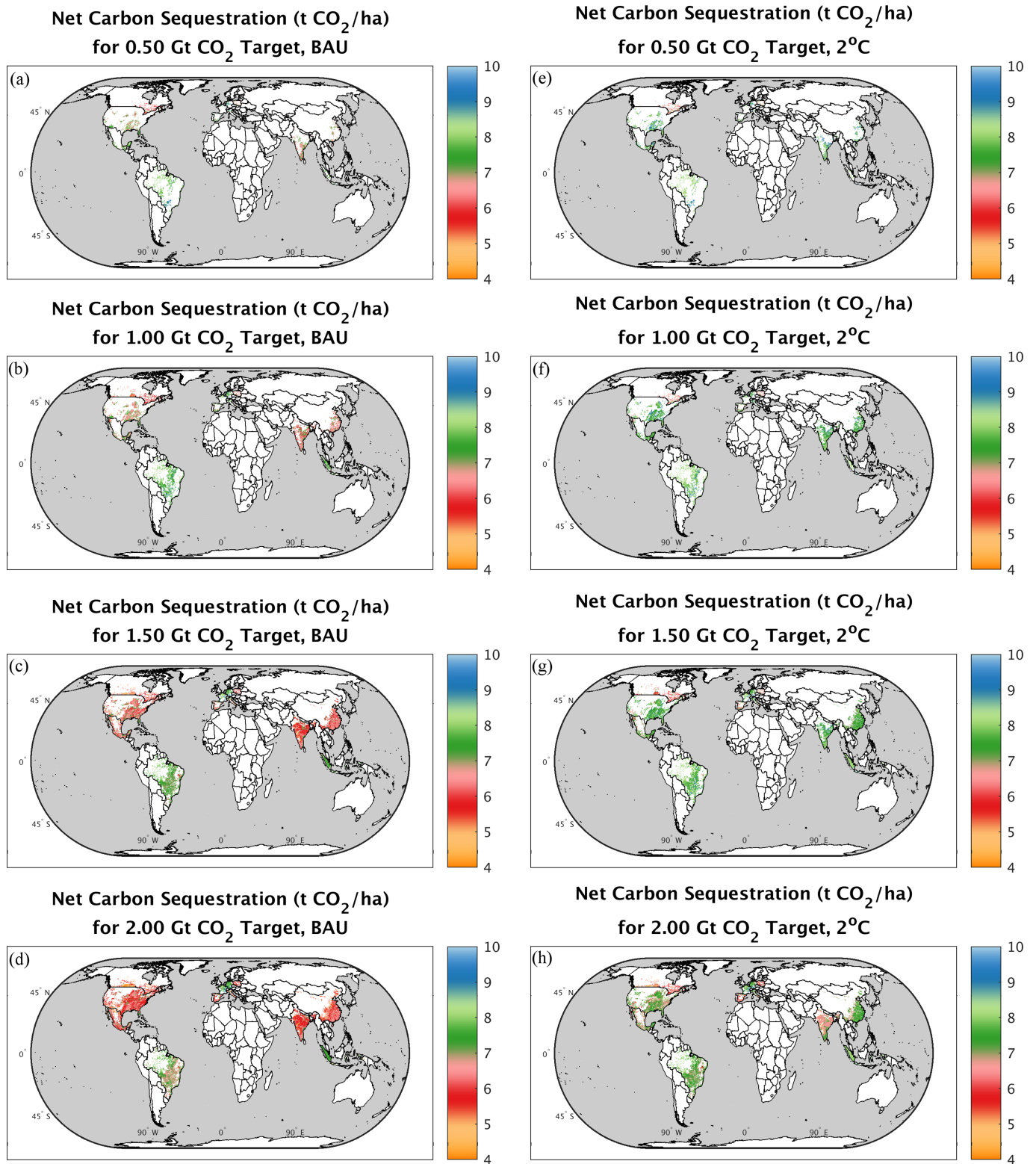
Simplified schematic overview
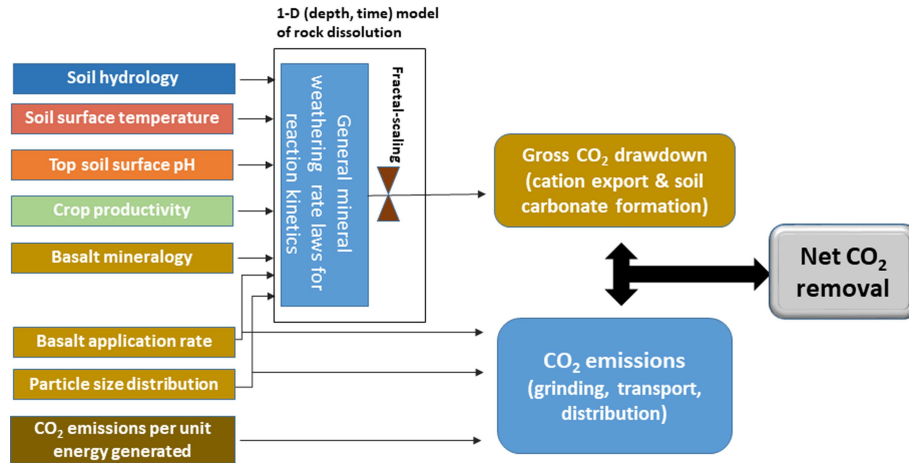
Extended Data Fig. 1 | Performance model schematic. Detailed methods are provided in Methods sections 'CDR simulation framework' and 'Model advances'. Spatially resolved key drivers are mapped in Extended Data Fig. 8; sources given in Supplementary Table 14.
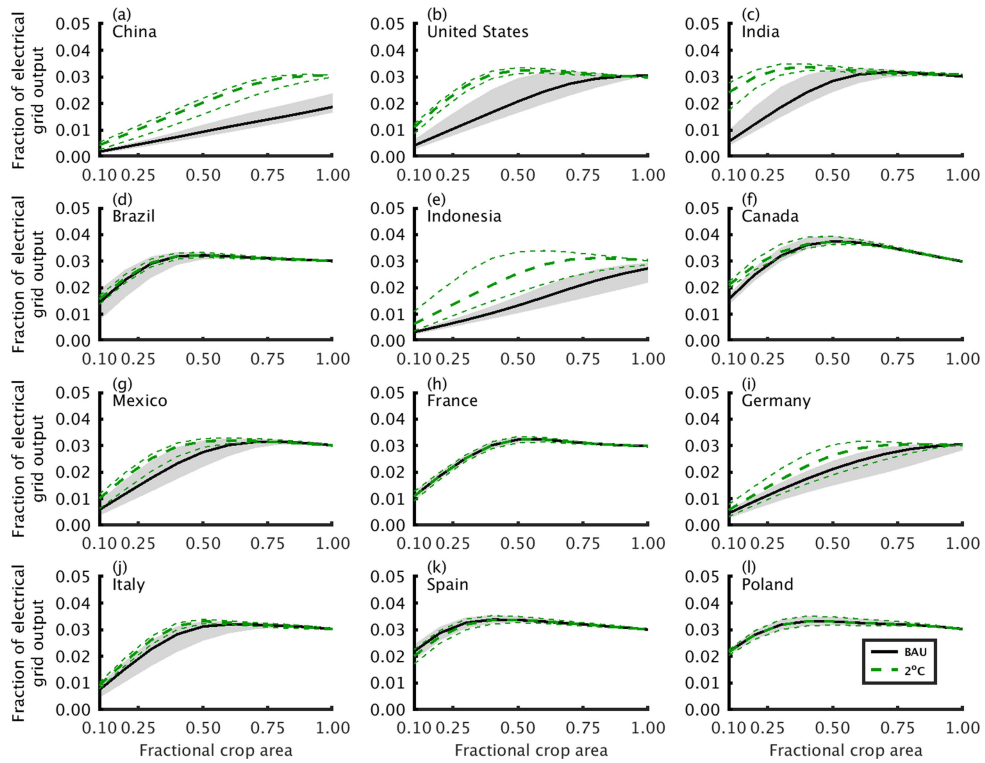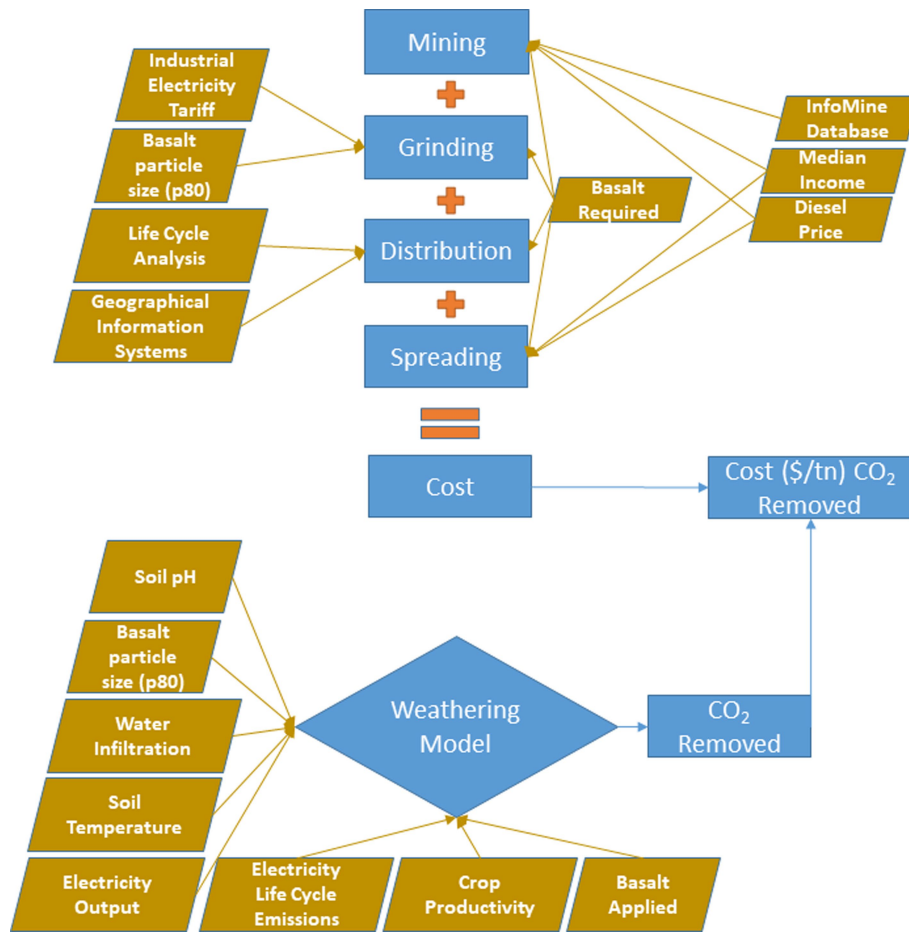
Extended Data Fig. 2 | Cumulative energy demand for rock grinding by nation. Results are shown for the top seven nations of the world (**a**–**g**), and the top five European nations (**h**–**l**), as ranked by net CDR capacity, with increasing fractional cropland area of ERW deployment. Curves depict simulations for the BAU and 2 °C energy policy scenarios. The grey-shaded area for each nation represents the 90% confidence interval calculated for basalts with relatively slow- versus fast-weathering rates for the BAU scenario; short green dashed lines indicate the 90% confidence limits of the corresponding 2 °C scenario simulations.

Net Carbon Sequestration (t CO$_2$/ha)
for 0.50 Gt CO$_2$ Target, BAU

Net Carbon Sequestration (t CO$_2$/ha)
for 0.50 Gt CO$_2$ Target, 2°C

Net Carbon Sequestration (t CO$_2$/ha)
for 1.00 Gt CO$_2$ Target, BAU

Net Carbon Sequestration (t CO$_2$/ha)
for 1.00 Gt CO$_2$ Target, 2°C

Net Carbon Sequestration (t CO$_2$/ha)
for 1.50 Gt CO$_2$ Target, BAU

Net Carbon Sequestration (t CO$_2$/ha)
for 1.50 Gt CO$_2$ Target, 2°C

Net Carbon Sequestration (t CO$_2$/ha)
for 2.00 Gt CO$_2$ Target, BAU

Net Carbon Sequestration (t CO$_2$/ha)
for 2.00 Gt CO$_2$ Target, 2°C

Extended Data Fig. 3 | Simulated net CDR with croplands via ERW. Net rates of CO$_2$ sequestration on croplands (annual and perennial combined) for the four targeted global CDR rates, 0.5 Gt CO$_2$ yr^{-1}, 1.0 Gt CO$_2$ yr^{-1}, 1.5 Gt CO$_2$ yr^{-1} and 2.0 Gt CO$_2$ yr^{-1} (Table 1) for the BAU (**a**–**d**) and the 2 °C (**e**–**h**) energy policy scenarios.

Extended Data Fig. 4 | Schematic overview of the environmental economics model. Interactions between the performance model, calculating net CDR, and the major components of the environmental economic model. Spatially resolved key drivers are mapped in Extended Data Fig. 9; sources given in Supplementary Table 14. Brown shading denotes inputs; blue shading denotes processes.
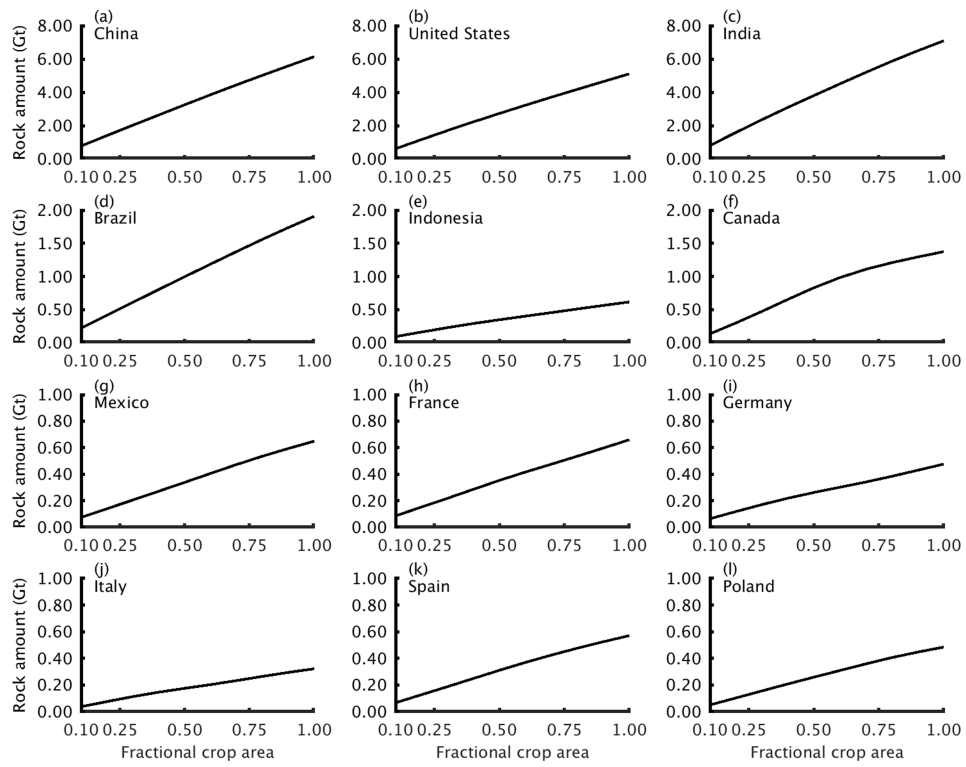
Extended Data Fig. 5 | Cumulative silicate demand by nation. Results are shown for the seven nations of the world (**a**–**g**) and the five European nations (**h**–**l**) with the highest CDR, as ranked by net CDR capacity, with increasing fractional cropland area deployment of ERW. Note the *y*-axis scale changes for European countries. Curves are the same irrespective of energy policy scenario.
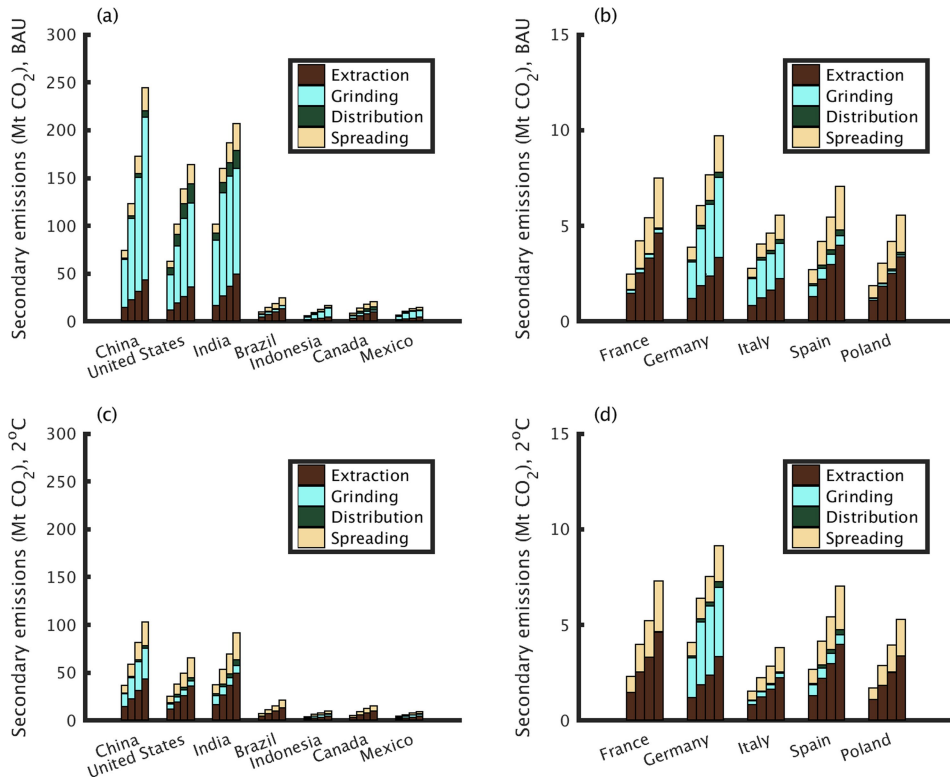
Extended Data Fig. 6 | Secondary CO$_2$ emissions from logistical ERW operations in 2050. a–d, Results are shown for the seven nations of the world (**a**, **c**) and the five European nations (**b**, **d**) with the highest CDR potential for the BAU scenario (**a**, **b**) and for the 2 °C energy policy scenario (**c**, **d**). For each country, from left to right, bars are for fractions of 0.25, 0.5, 0.75 and 1.0 of ERW deployment on croplands. Under the BAU scenario, CO$_2$ emissions from grinding dominate secondary emissions associated with ERW, except for France, where low-carbon nuclear power dominates. Under the 2 °C energy policy scenario (**c** and **d**), secondary CO$_2$ emissions generally drop for most nations as they transition to low-carbon energy sources in 2050 and implement negative emissions.
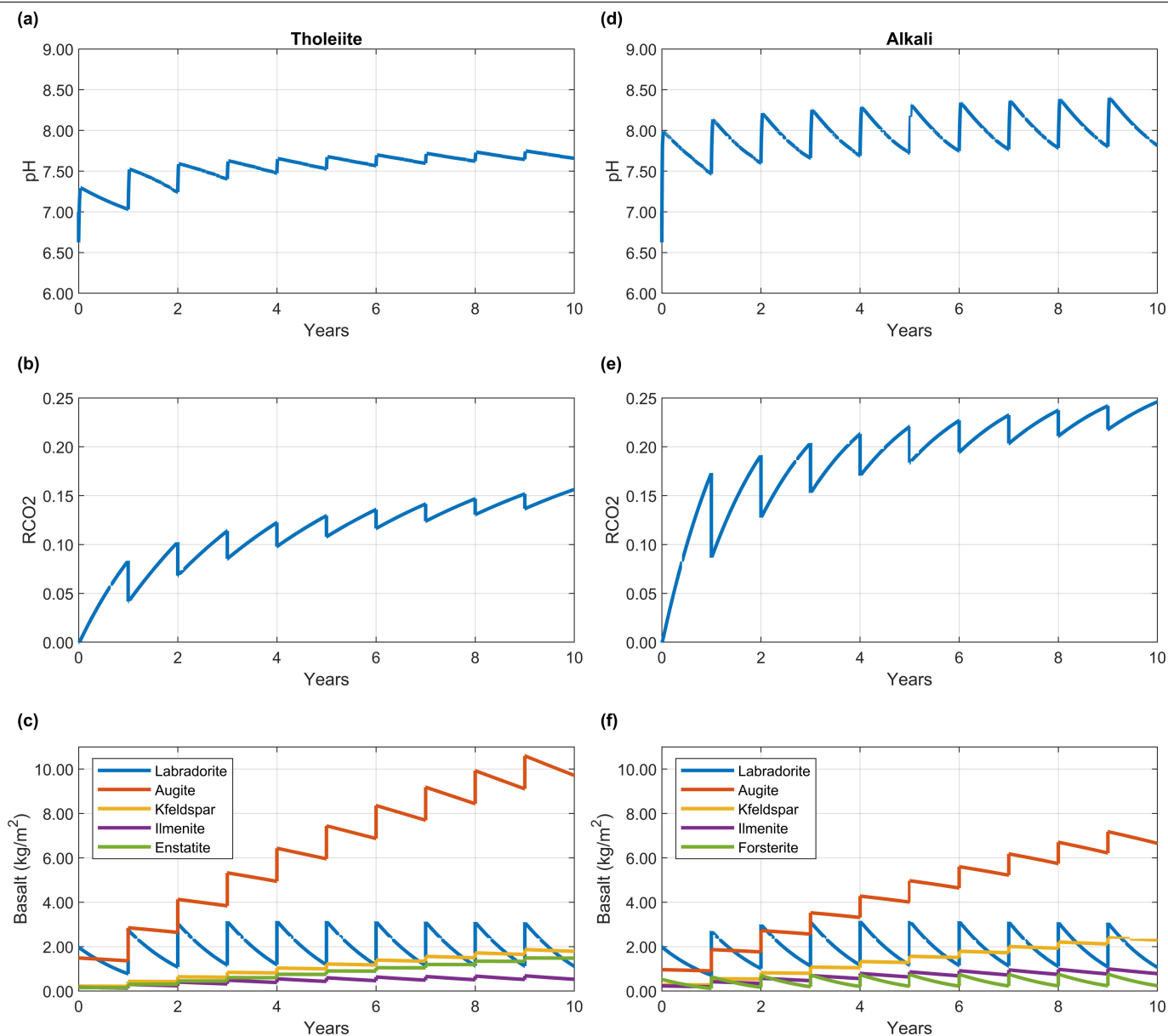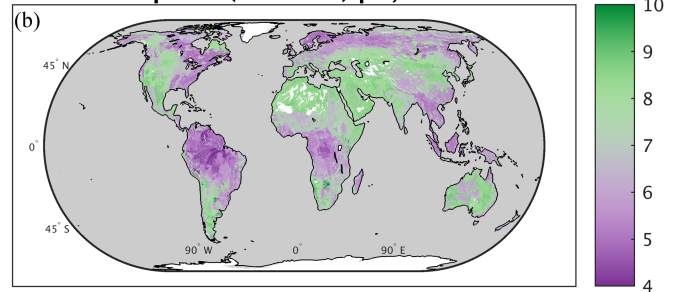
Extended Data Fig. 7 | Multi-year performance model simulations of weathering. Illustrative multi-year simulations of annual basalt application with the performance model showing the effects on soil pH, average efficiency of CDR (RCO_2), and soil mineral masses over a 10-year time horizon. **a**–**c**, pH, RCO_2 and mineral mass results for the tholeiitic basalt, respectively. **d**–**f**, pH, RCO_2 and mineral mass results for the alkali basalt (Supplementary Tables 1–3). All simulations used the same p80 particle size (100 μm) and were undertaken at 20 °C. Multi-year simulations capture the effect of basaltic minerals undergoing dissolution at different rates, with some minerals continuing to undergo dissolution and capture CO_2 after the first year of application. Such simulations allow average rates of weathering and CDR from repeated basaltic rock dust applications to be computed. Our extended theory underpinning the simulation framework tracks cohorts of particles applied each year and their mineral composition over time to account for cumulative effects (Supplementary Methods).
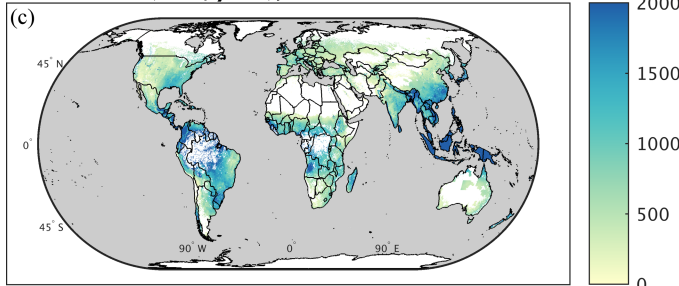
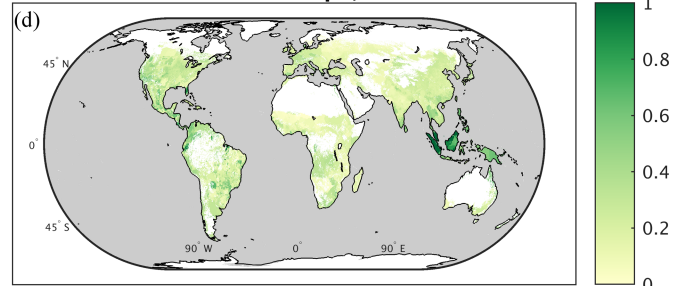**Soil Temperature (°C), 0–0.05 m RCP 8.5, 2050**
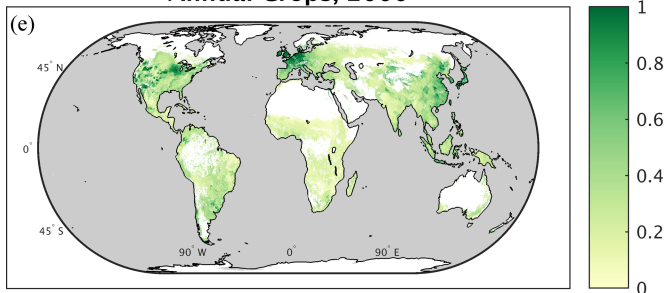
(a)
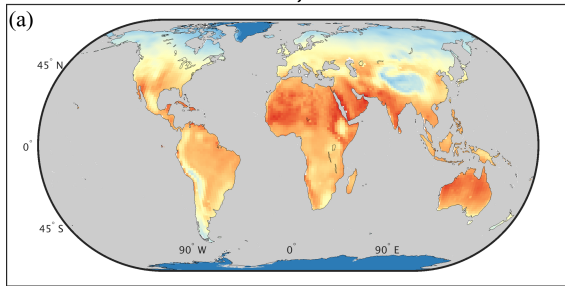
Top Soil (0–30 cm) pH, 2012

(b)

Water Infiltration in crops (mm/year), 1998–2002

(c)

**Net Primary Production Scaling Perennial Crops, 2000**

(d)

**Net Primary Production Scaling Annual Crops, 2000**

(e)

Extended Data Fig. 8 | Spatially resolved drivers of the performance model. **a**, Soil temperature from the Hadley Centre coupled Earth System Model (HadGEM) RCP 8.5 simulation for 2050 (the worst-case scenario). **b**, The HYDE harmonized soil pH database. **c**, Annual cropland soil water infiltration (irrigation water + precipitation minus evapotranspiration). **d**, **e**, Net primary production index for perennial and annual crops as derived from FAO datasets, respectively. Data sources and spatial resolution are specified in Supplementary Table 14.
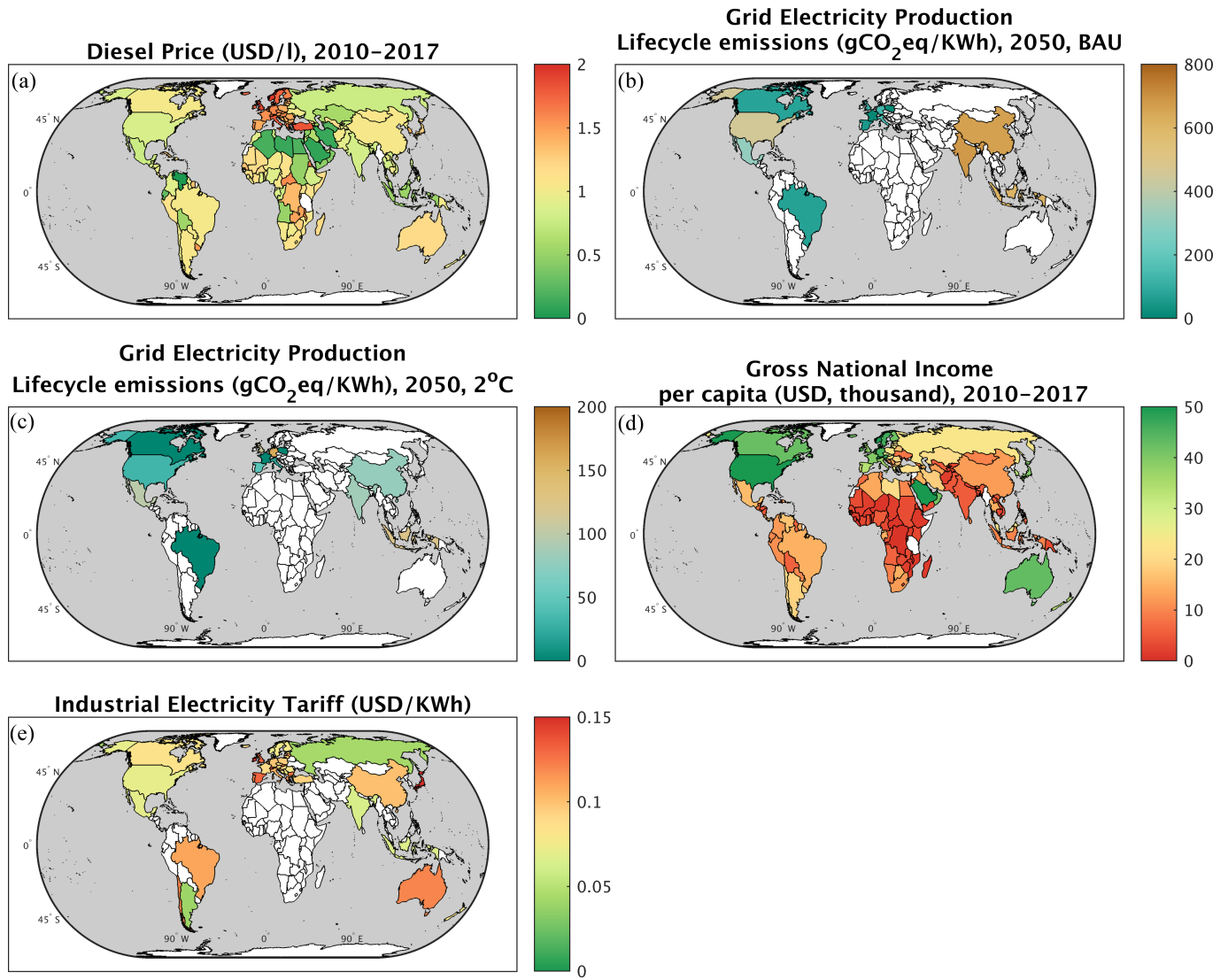
Extended Data Fig. 9 | Spatially resolved drivers for environmental economics modelling. a, Industrial diesel prices. **b**, **c**, CO_2 emissions intensity for the BAU scenario (**b**) and the 2 °C scenario (**c**). **d**, Gross national income per capita. **e**, Industrial electricity prices. Data sources and spatial resolution are specified in Supplementary Table 14.
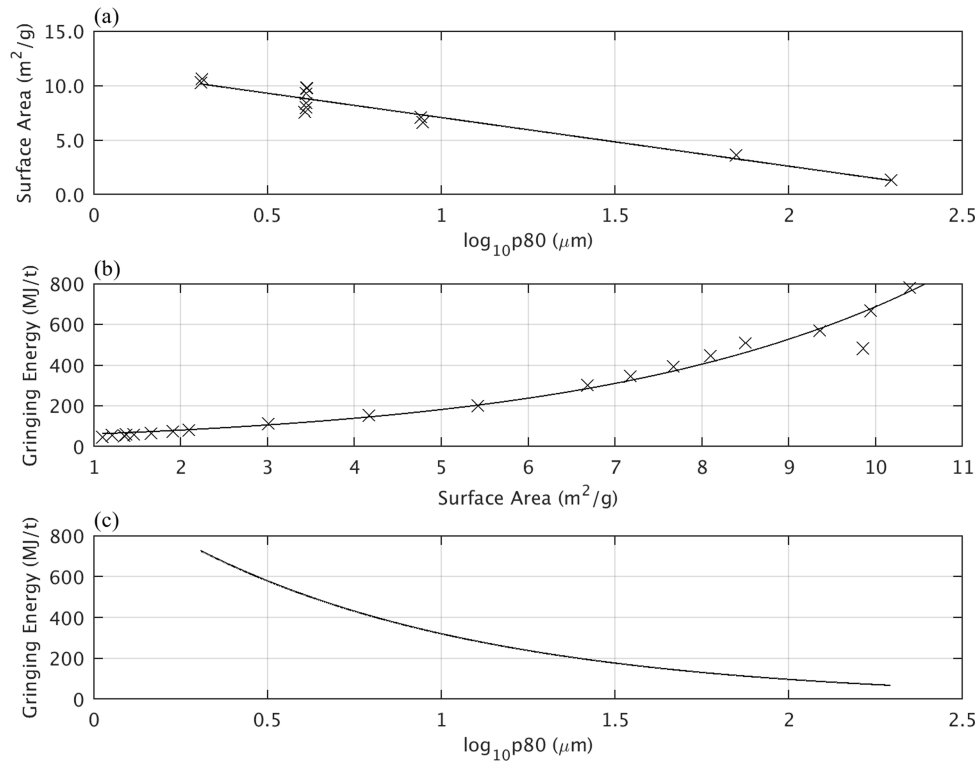
Extended Data Fig. 10 | Relationship between particle size, surface area and grinding energy. a, Relationship between particle size and surface area. **b**, Relationship between surface area and grinding energy. **c**, Relationship between particle size and grinding energy. p80 is defined as 80% of the particles having a diameter less than or equal to the specified size. Derived from data in ref. [73].